
# Effect of conduction band potential on cocatalyst-free plasmonic H2 evolution over Au loaded on Sr2+-doped CeO2

| | |
|---|---|
| Journal: | *Catalysis Science & Technology* |
| Manuscript ID | CY-ART-04-2019-000673.R1 |
| Article Type: | Paper |
| Date Submitted by the Author: | 16-May-2019 |
| Complete List of Authors: | Fudo, Eri; Kinki Daigaku<br>Tanaka, Atsuhiro; Kinki Daigaku<br>Kominami, Hiroshi; Kinki Daigaku |
| | |

PAPER

# Effect of conduction band potential on cocatalyst-free plasmonic $H_2$ evolution over Au loaded on $Sr^{2+}$-doped $CeO_2$

Received 00th January 20xx,
Accepted 00th January 20xx

DOI: 10.1039/x0xx00000x

Eri Fudo, [a] Atsuhiro Tanaka [b, c] and Hiroshi Kominami* [b]

There is little information on the effect of the conduction band (CB) position on plasmonic hydrogen ($H_2$) formation under visible light irradiation over gold (Au) nanoparticles supported on semiconductors because there were no appropriate materials of which the CB position gradually changes. In this study, we analyzed the flatband potential of strontium ion ($Sr^{2+}$)-doped cerium(IV) oxide ($CeO_2$:Sr) and found that the CB position gradually shifted negatively from +0.031 V to –1.49 V vs. NHE with an increase in the $Sr^{2+}$ mole fraction. Plasmonic photocatalysts consisting of Au nanoparticles, $CeO_2$:Sr and a platinum (Pt) cocatalyst were prepared and characterized by using X-ray diffraction, UV-vis spectroscopy, and transmission electron spectroscopy. Photocatalytic reaction under visible light irradiation revealed that $H_2$ was produced over Au nanoparticles supported on $CeO_2$:Sr having the CB potential of –0.61 V vs. NHE and that the negative limit of the CB position for electron injection from Au nanoparticles existed between –0.61 V and –1.49 V vs. NHE. We found that Au/$CeO_2$:Sr plasmonic photocatalysts also produced $H_2$ without the aid of a Pt cocatalyst due to the sufficiently negative potential of electrons injected into the CB of $CeO_2$:Sr.

## Introduction

Substance conversion using a photocatalyst is an important approach for solving or minimizing environmental and energy issues caused by mass consumption of fossil fuels. Titanium dioxide ($TiO_2$) is one of the most well-known photocatalysts that respond to ultraviolent (UV) light. UV light accounts for only about 5% of the total solar energy, while visible light accounts for about 50% of the solar energy. Therefore, the development of photocatalysts that respond to visible light and photocatalytic substance conversion are important from the viewpoint of efficient utilization of solar energy. One of the most attractive approaches for the development of a visible light-responding photocatalyst is the surface modification method (SMM)[1]. Various surface modifiers have been reported, and it has been shown that $TiO_2$ modified with a platinum complex[2a], rhodium ion[2b], copper ion[3], organic compounds[4] and plasmonic particles[5-10] induced photocatalytic reactions under visible light irradiation. In these photocatalysts, electrons of the modifier were transferred to the conduction band (CB) of $TiO_2$[2,4,5-10] or electrons of the valence band (VB) of $TiO_2$ were transferred to the modifier[3]. A unique point of the SMM method is that characteristics of the photocatalysts such as photoabsorption properties, redox properties and adsorption properties can be controlled by properties of the surface modifier introduced on $TiO_2$.

Some metal nanoparticles (gold (Au), silver and copper) show strong photoabsorption in a visible light region due to surface plasmon resonance (SPR). Since Au nanoparticles are the most stable nanoparticles in water and air atmosphere among these metals, Au nanoparticles have been applied to the fields of catalysis chemistry and biochemistry. In 2009, Kowalska *et al.*[5] reported that Au nanoparticles supported on $TiO_2$ (Au/$TiO_2$) worked as a photocatalyst under irradiation of visible light (λ = *ca.* 550 nm) in oxidation of 2-propanol. After their work, there have been many reports of Au-metal oxide materials working as visible-light-responding photocatalysts, *i.e*, plasmonic photocatalysts, for various chemical reactions such as decomposition of organic substrates[6], selective oxidation of an aromatic alcohol to a carbonyl compound[7], $H_2$ formation from alcohols[8], reduction of organic compounds[7c, 9] and water splitting[10]. In most of those reports, electron injection from Au nanoparticles to the CB of semiconductors has been proposed as the reaction mechanism[5-10]. It has also been reported that cerium(IV) oxide ($CeO_2$)[6b,6c], g-$C_3N_4$[11], $WO_3$[12] and $BiVO_4$[13] can be used as supporting materials of Au nanoparticles and that hot electrons were injected to the supporting materials. However, as far as we know, there has been no study in which the effect(s) of the position of the CB

[a] *Department of Molecular and Material Engineering, Graduate School of Science and Engineering Kindai University, 3-4-1 Kowakae, Higashiosaka, Osaka 577-8502, Japan.*
[b] *Department of Applied Chemistry, Faculty of Science and Engineering Kindai University, 3-4-1 Kowakae, Higashiosaka, Osaka 577-8502, Japan.*
[c] *Precursory Research for Embryonic Science and Technology (PRESTO), Japan Science and Technology Agency (JST), 4-1-8 Honcho, Kawaguchi 332-0012, Japan*
*E-mail: hiro@apch.kindai.ac.jp*
Electronic Supplementary Information (ESI) available: Figs. 1-5 and Table S1. See DOI: 10.1039/x0xx00000x

of semiconductors on catalytic performance of an Au plasmonic photocatalyst was investigated because there are no appropriate materials of which the position of the CB gradually changes. Therefore, there is little information about the negative limit of the CB position for electron injection from Au nanoparticles induced by SPR under visible light irradiation.

For photcatalytic $H_2$ production over plasmonic photocatalysts, the position of the CB ($E_{CB}$) of the supporting materials must be more negative than the potential of $H^+$ reduction (0 V vs. NHE) because hot electrons are injected into the CB. Introduction of a precious metal such as platinum (Pt) as a cocatalyst is indispensable for $H_2$ formation over Au-$TiO_2$ plasmonic photocatalysts[8c,8d] as well as $TiO_2$ photocatalysts because the $E_{CB}$ of $TiO_2$ (-0.2 V vs. NHE, pH=0[14]) is very close to the potential of $H_2$ evolution. If the $E_{CB}$ of supporting materials is sufficiently more negative than the potential of $H^+$ reduction, cocatalyst-free $H_2$ evolution over Au plasmonic photocatalysts would be possible.

In the present study, we investigated the negative limit of the CB position for electron injection from Au nanoparticles in a plasmonic photocatalyst under visible light irradiation. For this study, we used strontium ion ($Sr^{2+}$)-doped $CeO_2$ ($CeO_2$:Sr) having various $Sr^{2+}$ mole fractions as the supporting material of Au, because a new band was created at a negative position of the Ce 5d band by hybridization with an Sr 5s5p orbital[15, 16], and then we determined the position of the CB by an electrochemical technique. We also examined $H_2$ evolution over Au/$CeO_2$:Sr with and without a Pt cocatalyst under visible light irradiation and found that Au/$CeO_2$:Sr produced $H_2$ without the aid of a cocatalyst.

## Experimental

### 2.1 Preparation of $CeO_2$:Sr having various $Sr^{2+}$ mole fractions

$CeO_2$:Sr was prepared according to a previous study:[15] $CeO_2$ (Kanto chemical, Tokyo-Nano tek®) and $SrCO_3$ (Wako Chemicals, Tokyo) were mixed with various $Sr^{2+}$ mole fractions and the mixtures were calcined in air at 1273 K for 10 h. The mole fractions, x (= Sr / (Sr + Ce)), were changed from 0 ($Sr^{2+}$-free) to 0.50 (equimolar). Hereafter, the samples obtained are designated as $CeO_2$:Sr(x).

### 2.2 Loading of a platinum (Pt) co-catalyst on $CeO_2$:Sr

Loading of 0.5 wt% Pt nanoparticles on $CeO_2$:Sr (preparation of $CeO_2$:Sr-Pt) was performed by the photodeposition (PD) method. $CeO_2$:Sr powder was suspended in 10 $cm^3$ of an aqueous solution of methanol (50 vol%) in a test tube, and the test tube was sealed with a rubber septum under argon (Ar). An aqueous solution of hexachloroplatinic acid ($H_2PtCl_6$) as the Pt source was injected into the sealed test tube and then the mixture was photoirradiated for 1 h at λ> 300 nm by a 400 W high-pressure mercury arc (Eiko-sha, Osaka) with magnetic stirring in a water bath continuously kept at 298 K. The Pt source was reduced by photogenerated electrons, and Pt metal particles were deposited on the surface of $CeO_2$:Sr particles. Analysis of the liquid phase after photodeposition revealed that the Pt source had been almost completely (>99.9%) deposited on the $CeO_2$:Sr particles. The resultant powder was washed repeatedly with distilled water and then dried at 293 K in vacuo for 2 h.

### 2.3 Loading of Au particles on $CeO_2$:Sr-Pt

As the first step, colloidal Au nanoparticles to be loaded on $CeO_2$:Sr-Pt were prepared using the method reported by Frens[17]. To 750 $cm^3$ of an aqueous tetrachloroauric acid ($HAuCl_4$) solution (0.49 mmol $dm^{-3}$), 100 $cm^3$ of an aqueous solution containing sodium citrate (39 mmol $dm^{-3}$) was added. The solution was heated and boiled for 1 h. After the color of the solution had changed from deep blue to deep red, the solution was boiled for an additional 30 min. After the solution had been cooled to room temperature, Amberlite MB-1 (ORGANO, 60 $cm^3$) was added to remove excess sodium citrate. After 10 min of treatment, MB-1 was removed from the solution using a glass filter.

As the second step, loading of Au on $CeO_2$:Sr-Pt (preparation of Au/$CeO_2$:Sr-Pt) was performed by colloid photodeposition with a hole scavenger method (CPH)[6e]. Preparation of $CeO_2$:Sr-Pt having 1.0 wt% Au is described as a typical sample. $CeO_2$:Sr-Pt powder was suspended in 20 $cm^3$ of an aqueous solution of colloidal Au nanoparticles in a test tube, and the test tube was sealed with a rubber septum under Ar. After an aqueous solution of oxalic acid (50 μmol) had been injected into the sealed test tube, the mixture was photoirradiated at λ> 300 nm by a 400 W high-pressure mercury arc with magnetic stirring in a water bath continuously kept at 298 K. The resultant powder was washed repeatedly with distilled water and then dried at 293 K in vacuo for 2 h.

### 2.4 Characterization

X-ray diffraction (XRD) patterns of the samples were recorded using a Rigaku Multi Flex (Cu Kα, 40 V, 30 mA) with a carbon monochromator. Diffraction patterns were obtained in the angle range from 10° to 90°. Diffuse reflectance spectra of the samples were obtained with a UV-vis spectrometer (UV-2600, Shimadzu, Kyoto) equipped with a diffuse reflectance measurement unit (ISR-2600PLUS, Shimadzu) in which barium sulfate ($BaSO_4$) was used as a reference. Morphology of the samples was observed under a JEOL JEM-3010 transmission electron microscope (TEM) operated at 300 kV in the Joint Research Center of Kindai University.

### 2.5 Photocatalytic hydrogen ($H_2$) evolution

The dried photocatalyst powder (50 mg) was suspended in an aqueous 2-propanol solution (10 vol%, 5 $cm^3$), bubbled with Ar, and sealed with a rubber septum. The suspension was irradiated with visible light of a 500 W xenon (Xe) lamp (Ushio, Tokyo) filtered with a Y-48 filter (AGC Techno Glass, Shizuoka) (450−800 nm: 150 mW $cm^{-2}$) with magnetic stirring in a water bath continuously kept at 298 K. The amount of $H_2$ in the gas phase was measured using a GC-8A gas chromatograph (Shimadzu, Kyoto) equipped with an MS-5A column. The amount of acetone in the liquid phase was determined with a GC-14A gas chromatograph (Shimadzu) equipped with a fused-silica capillary column (HiCap-CBP20, 25 m, 0.22 mm). Toluene was used as an internal standard sample. The reaction solution (1 $cm^3$) was added to a diethyl ether/water mixture (2:1 v/v, 3 $cm^3$). After the mixture had been stirred for 10 min, acetone in the ether phase was analyzed. The amount of acetone was

determined from the ratio of the peak area of acetone to the peak area of toluene.

### 2.6 Electrode preparation and impedance measurement

To evaluate electrochemical properties of $CeO_2$:Sr, an electrode consisting of $CeO_2$:Sr powder was prepared by using an electrophoretic deposition method. In acetone (80 $cm^3$, Wako, 99.0%) containing iodine (16 mg, Wako, 99.0%), $CeO_2$:Sr powder (100 mg) was suspended under sonication for 10 min. Two fluorine-doped tin oxide (FTO, 1.5×5 $cm^2$, AGC, Tokyo) electrodes were immersed in the solution with a distance between them of 1.0 cm, and 10 V of bias was applied for 10 min, during which $CeO_2$:Sr powder was deposited on the anodic substrate, resulting in the formation of $CeO_2$:Sr/FTO. Then the electrode was annealed at 200°C for 1 h.

Impedance measurements were done in a three-electrode electrochemical cell using $CeO_2$:Sr/FTO, Ag/AgCl, and Pt wire as the working electrode, reference electrode, and counter electrode, respectively. An aqueous $Na_2SO_4$ solution (0.1 M, pH 6) was used as an electrolyte. Before the measurements, the dissolved air was removed by purging with Ar gas for 30 min. The imaginary component of the impedance (Z'') of the equivalent circuit including the $CeO_2$:Sr/FTO electrode was evaluated at three current frequencies of 35.0 kHz, 43.0 kHz and 50.0 kHz with sweeping applied voltage from -0.85 to 0.75 V vs. Ag/AgCl using an electrochemical measurement system (HZ-7000, Hokuto Denko, Hyogo).

Flatband potential values from impedance measurements were obtained from the extrapolation of Mott-Schottky plots ($C^{-2}$ vs. applied potential) using the following equation (1):

$$\frac{1}{C^2} = \frac{2}{\varepsilon\varepsilon_0 A e N_D}\left(E - E_{FB} - \frac{k_B T}{e}\right) \quad (1)$$

where $C$ is the space capacitance (calculated from equation (2)), $\varepsilon$ is the dielectric constant of the semiconductor, $\varepsilon_0$ is the permittivity of free space, $A$ is the interfacial area, $N_D$ is the number of donors, $E$ is the externally applied potential, $E_{FB}$ is the flatband potential at the semiconductor/electrolyte junction, $k_B$ is Boltzmann's constant, $T$ is the absolute temperature, and $e$ is the electronic charge,

$$|Z''| = \frac{1}{2\pi f C} \quad (2)$$

The difference in the potential ($E$) derived from the pH value of the electrolyte solution was revised in accordance with the Nernst equation (3):

$$E(\mathrm{pH} = a) = E(\mathrm{pH} = b) - 0.059 \times (a - b) \quad (3)$$

The potential (vs. Ag/AgCl) was converted to the potential (vs. NHE) by the following equation (4):

$$E(vs.\,\mathrm{NHE}) - E(vs.\mathrm{Ag/AgCl}) = 0.199\ \mathrm{V} \quad (4)$$

## Results and discussion

### 3.1 Characterization of $CeO_2$ powder and $CeO_2$:Sr powder

Figure 1 shows Mott-Schottky plots of $CeO_2$:Sr(x)/FTO based on the impedance measurements. As Chun[18] and Iguchi[19] mentioned, the flatband potential ($E_{FB}$) values of semiconductors were determined from intersection points of the plots and the x-axis. Mott-Schottky plots of $CeO_2$:Sr(0.25) and fitted lines derived from impedance measurements at different frequencies are shown in Figure 1(a)-(c). Generally, all of the fitted lines of Mott–Schottky plots obtained at different frequencies should converge on the same $E_{FB}$ ($C^{-2}$ = 0). As shown in Figure 1 (a)-(c), three fitted lines of $CeO_2$:Sr(0.25) converged on $E_{FB}$= –0.36 V. Mott-Schottky plots of other samples determined at 50.0 kHz are also shown in Figure 1. The slopes of their fitted lines were positive, indicating that $CeO_2$ and $CeO_2$:Sr(x) are n-type semiconductors. The $E_{FB}$ values of $CeO_2$:Sr(x) calculated from the Mott-Schottky plots are shown in Figure 2. The $E_{FB}$ values of $CeO_2$:Sr(x) shifted negatively and almost linearly with an increase in x up to x= 0.40. $E_{FB}$ of $CeO_2$:Sr(0.50) was more negative than that expected from the linearity. Since the Fermi level of n-type semiconductors is considered to merge with the lowest potential of the conduction band[20], $E_{FB}$ calculated from the impedance measurement can be regarded as the value of $E_{CB}$. This means that $CeO_2$:Sr samples having different $E_{CB}$ were successfully prepared by changing x of $CeO_2$:Sr(x).

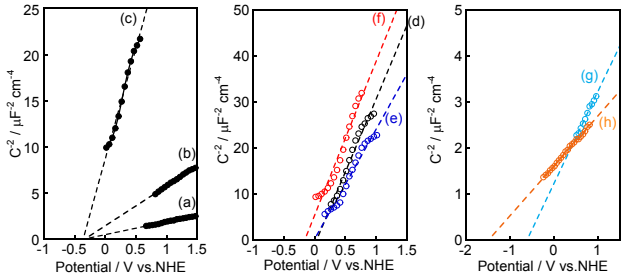


Figure 1 Mott-Schottky plots based on the results of impedance measurements. Plots for $CeO_2$:Sr(0.25)/FTO at frequencies of (a) 35.0 kHz , (b) 43.0 kHz and (c) 50.0 kHz. Plots for (d) $CeO_2$/FTO, (e) $CeO_2$:Sr(0.050)/FTO and (f) $CeO_2$:Sr(0.10)/FTO at a frequency of 50.0 kHz. Plots for (g) $CeO_2$:Sr(0.40)/FTO and (h) $CeO_2$:Sr(0.50)/FTO at a frequency of 50.0 kHz.

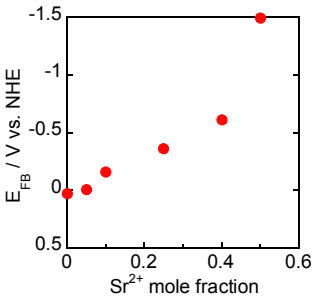


Figure 2 Effect of $Sr^{2+}$ mole fraction (x) on flatband potential ($E_{FB}$) of $CeO_2$:Sr(x).

Figure 3 shows XRD patterns of $CeO_2$ and $CeO_2$:Sr(x) with various $Sr^{2+}$ mole fractions. The commercially available $CeO_2$ (undoped $CeO_2$) had a fluorite structure (ICDD PDF#43-1002). In the case of $CeO_2$:Sr(x), diffraction peaks due to $CeO_2$ did not shift and additional peaks assignable to $SrCeO_3$ (ICDD PDF#47-1689) were observed at $2\vartheta$= 29.5, 42.2, 52.6 and 60.6°. These results are consistent with the results reported by Kadowaki *et al.*[15] Yabe *et al*. prepared $Sr^{2+}$-doped $CeO_2$ *via* a soft solution chemical route and subsequent calcination at 1273 K and determined the solubility limit of SrO to be x= 0.10[21]. The

results obtained by the two research groups are slightly different, *i.e.*, no $Sr^{2+}$ can be doped to $CeO_2$, while $Sr^{2+}$ can be doped until x= 0.10. The different results were probably caused by the different methods used for $Sr^{2+}$ doping (solid state reaction vs. soft chemical reaction) and both groups observed the formation of $SrCeO_3$. In any case, the no or low solubility of SrO may be attributed to the large difference in the ionic size of $Sr^{2+}$ from that of $Ce^{4+}$. However, it is difficult to explain the gradual changes of $E_{CB}$ of $CeO_2$:Sr(x) by the two structures and the ratio of $CeO_2$ and $SrCeO_3$ because the $E_{CB}$ is determined by the properties of one compound. One possible explanation of the gradual change is that $Sr^{2+}$ doping with wide fractions occurred in the outermost surface of product particles with several nanometers,[15] which was not detected with the XRD method. A similar case was recently reported in $Sm^{3+}$ doping to $CeO_2$ by using a solid state reaction[22]. In other words, the surface of $CeO_2$ particles was modified with $Sr^{2+}$, resulting in the formation of Ce-Sr-O phases having physical properties different from those of $CeO_2$. This structure probably prevented the electron transfer from the CB of $CeO_2$:Sr(x) to that of $CeO_2$ present inside the particles. In the DFT calculation for $Sr^{2+}$-doped $CeO_2$, the occupied valence band was composed of an O2p orbital and a Ce5d orbital hybridized with Sr5s5p orbitals, appearing over the unoccupied band consisting of a Ce4f orbital[16]. We have not been able to obtain clear structural information on the surface phase(s), although X-ray photoelectron spectroscopy of $CeO_2$:Sr(x) indicated the presence of Sr species having a binding energy (132.6 eV) at the surface, the binding energy being similar to that of Sr species in strontium oxide (SrO) (132.6 eV) (Figure S1, †ESI)[23].

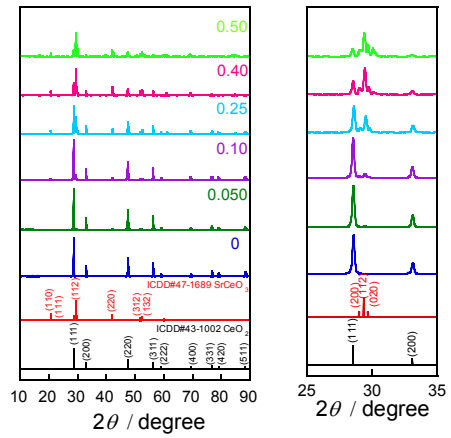


Figure 3 XRD patterns of $CeO_2$ (undoped, x= 0) and $CeO_2$:Sr(x) with different mole fractions (x= 0.050, 0.10, 0.25, 0.40 and 0.50).

Figure 4 shows TEM images of (a) $CeO_2$:Sr(0.25), (b) $CeO_2$:Sr(0.25)-Pt(0.5), (c) Au(1.0)/$CeO_2$:Sr(0.25) and (d) Au(1.0)/$CeO_2$:Sr(0.25)-Pt(0.5). Figure 4(a) shows that $CeO_2$:Sr(0.25) consisted of large particles with an average diameter of 100 nm; however, no change was observed at the outermost surface of the particles. Fine particles were observed in the TEM image of $CeO_2$:Sr(0.25)-Pt (Figure 4(b)) and the average diameter was determined to be 2.8 nm (Figure S2(a), †ESI), indicating that the Pt nanoparticles were successfully deposited on the surface of $CeO_2$:Sr(0.25) particles by the PD method. Figure S3 (†ESI) shows a TEM image and distribution of colloidal Au nanoparticles. The Au nanoparticles had an average size of 13 nm within a relatively sharp distribution with a standard deviation of 1.4 nm. A TEM image of Au(1.0)/$CeO_2$:Sr(0.25) (Figure 4(c)) shows that Au nanoparticles were successfully deposited on the surface of $CeO_2$:Sr(0.25) particles by the CPH method. The average diameter of Au particles was determined to be 13 nm (Figure S2(b), †ESI), which is in good agreement with the average diameter of the original colloidal Au nanoparticles (Figure S3, †ESI). Two types of particles having different sizes were observed in the TEM image of Au(1.0)/$CeO_2$:Sr(0.25)-Pt(0.5) (Figure 4(d)) and the average sizes of the two types of particles were determined to be 2.9 nm and 13 nm (Figure S4, †ESI). From the TEM images of $CeO_2$:Sr(0.25)-Pt and Au(1.0)/$CeO_2$:Sr(0.25), the smaller and larger particles of Au(1.0)/$CeO_2$:Sr(0.25)-Pt(0.5) were assigned to Pt particles and Au particles, respectively. These results show that Au particles were successfully loaded on $CeO_2$:Sr(0.25)-Pt(0.5) without change in the original sizes of both Au particles and Pt particles during loading of Au particles. Since $CeO_2$:Sr(x) was prepared under the same condition, the surface area was almost the same, suggesting that properties of $CeO_2$:Sr(x) other than the CB position are almost same and their effects on the catalytic performance would be negligible. Figure S5 (†ESI) shows UV-vis spectra of $CeO_2$:Sr(0.25) and Au/$CeO_2$:Sr(0.25), indicating that photoabsorprtion due to SPR of Au particles occurred at around 530 nm.

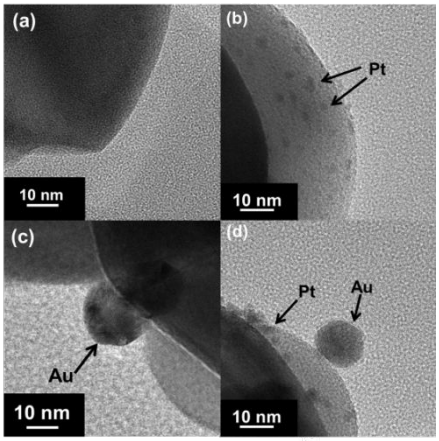


Figure 4 TEM photographs of (a) $CeO_2$:Sr(0.25), (b) $CeO_2$:Sr(0.25)-Pt(0.5), (c) Au(1.0)/ $CeO_2$:Sr(0.25) and (d) Au(1.0)/ $CeO_2$:Sr(0.25)-Pt(0.5).

### 3.2 Photocatalytic $H_2$ production over Au/$CeO_2$-Pt and Au/$CeO_2$:Sr(0.25)-Pt

By using the PD method, $CeO_2$ and $CeO_2$:Sr(0.25) were platinized and then Au particles were loaded on the platinized samples by using the CPH method. Thus-prepared Au(1.0)/$CeO_2$-Pt(0.5) and Au(1.0)/$CeO_2$:Sr(0.25)-Pt(0.5) were used for photocatalytic reaction of 2-propanol in aqueous suspensions under irradiation of visible light at 298 K, and the time courses of formation of $H_2$ and acetone are shown in Figure 5. No $H_2$ and acetone were produced over Au(1.0)/$CeO_2$-Pt(0.5) (Figure 5(a)). This result is explained by

the $E_{CB}$ of undoped $CeO_2$ (+0.031 V vs. NHE) determined by the impedance measurement, *i.e.*, the $E_{CB}$ of $CeO_2$ is insufficient for $H_2$ production (0 V vs. NHE) even though hot electrons are injected into the CB.

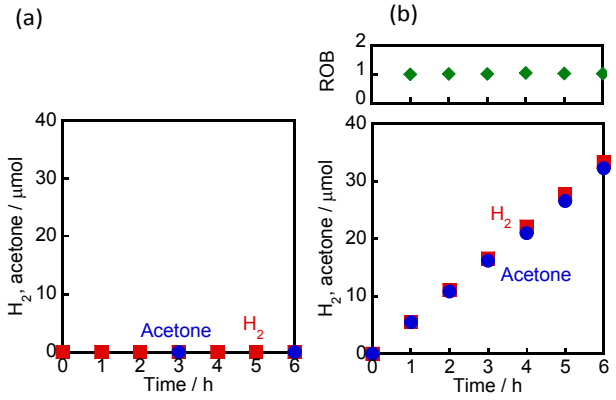


Figure 5 Time courses of formation of $H_2$ and acetone from 2-propanol over (a) Au/$CeO_2$-Pt and (b) Au(1.0)/$CeO_2$:Sr(0.25)-Pt(0.5) under irradiation of visible light from a Xe lamp with a Y48 cut filter.

In contrast to the results for Au(1.0)/$CeO_2$-Pt(0.5), $H_2$ was produced from suspensions of Au(1.0)/$CeO_2$:Sr(0.25)-Pt(0.5) under the same photoirradiation conditions (Figure 5(b)) and the yield of $H_2$ reached 33 μmol after photoirradiation for 6 h. The yield was larger than the amounts of Au (0.098 μmol) and Pt (0.049 μmol) loaded on $CeO_2$:Sr(0.25), indicating that $H_2$ was produced via a catalytic process. Some blank reactions were carried to understand the $H_2$ formation over Au(1.0)/$CeO_2$:Sr(0.25)-Pt(0.5) under visible light irradiation, and the results are summarized in Table S1 (†ESI). No $H_2$ was produced from 2-propanol in aqueous suspensions of $CeO_2$:Sr(0.25)-Pt(0.5) and $CeO_2$:Sr(0.25) under visible light irradiation (Entries 2 and 3), indicating that $CeO_2$:Sr(0.25) did not work as band-gap type photocatalyst under irradiation of visible light and that Au particles are indispensable for $H_2$ evolution under the conditions. No $H_2$ was evolved from an aqueous 2-propanol suspension of Au(1.0)/$CeO_2$:Sr(0.25)-Pt(0.5) in the dark (Entry 4), indicating that no thermal reaction occurred over Au(1.0)/$CeO_2$:Sr(0.25)-Pt(0.5) and that light irradiation is required for $H_2$ production under the present conditions. Light irradiation to an aqueous 2-propanol solution without any solid gave no $H_2$ (Entry 5), which means that no photochemical reaction took place under the present photoirradiation conditions. These blank reactions show that electrons were provided from Au particles under visible light irradiation, *i.e.*, Au(1.0)/$CeO_2$:Sr(0.25)-Pt(0.5) worked as plasmonic photocatalyst. The contrasting results for Au(1.0)/$CeO_2$-Pt(0.5) and Au(1.0)/$CeO_2$:Sr(0.25)-Pt(0.5) in $H_2$ evolution under visible light irradiation mean that the $E_{CB}$ is very important and that the $E_{CB}$ of $CeO_2$:Sr(0.25) (−0.36 V vs. NHE) is a key factor for $H_2$ production over Au(1.0)/$CeO_2$:Sr(0.25)-Pt(0.5). In other words, hot electrons were injected from Au particles into the CB of $CeO_2$:Sr(0.25) and used for $H_2$ evolution because the potential of electrons in the CB of $CeO_2$:Sr(0.25) is sufficient for $H_2$ production. Therefore, we conclude that Au(1.0)/$CeO_2$:Sr(0.25)-Pt(0.5) worked as a plasmonic photocatalyst. Production of $H_2$ over Au(1.0)/$CeO_2$:Sr(0.25)-Pt(0.5) provides another important piece of information: hot electrons can be injected into the CB that is located at −0.36 V vs. NHE under irradiation of visible light.

As the oxidized product, 33 μmol of acetone was formed by photoirradiation for 6 h, while no $CO_2$ was detected during the photoirradiation. Therefore, the overall photocatalytic reaction is expressed as Equation 5:

$$(CH_3)_2CHOH \rightarrow H_2 + (CH_3)_2CO \quad (5).$$

Redox balance (ROB) was calculated from Equation 6:

$$ROB = n(H_2) / n(\text{acetone}) \quad (6),$$

where $n(H_2)$ and n(acetone) are the amounts of $H_2$ and acetone produced during the photoirradiation, respectively. As also shown in Figure 5(b), the values of ROB were almost unity regardless of irradiation time. These results indicate that formation of $H_2$ and acetone from 2-propanol occurred with a high stoichiometry as shown in Equation 5.

### 3.3 Effect of $E_{CB}$ of $CeO_2$:Sr(x) on $H_2$ evolution over Au/$CeO_2$:Sr(x)-Pt

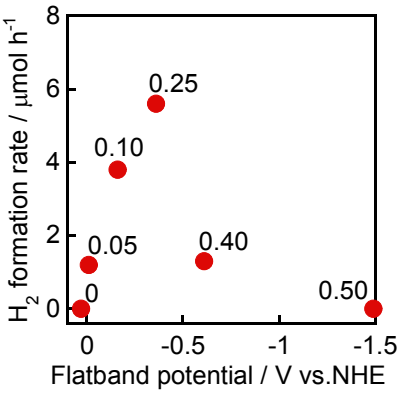


Figure 6 Effect of $E_{FB}$ on $H_2$ formation rate of an Au(1.0)/$CeO_2$:Sr(x)-Pt(0.5) plasmonic photocatalyst. Values in the figure show mole fractions of $Sr^{2+}$ (x).

Since $E_{FB}$ values (Figure 2) of $CeO_2$:Sr(x) gradually shifted negatively with an increase in x, a series of $CeO_2$:Sr(x) samples are suitable compounds to investigate the effect(s) of the $E_{CB}$ of the support for Au particles on plasmonic $H_2$ evolution under visible light irradiation. Figure 6 shows the effect of the $E_{CB}$ of $CeO_2$:Sr(x) on the rate of $H_2$ evolution. No $H_2$ was produced over Au(1.0)/$CeO_2$-Pt(0.5) due to the insufficient CB position of $CeO_2$ (+0.031 V vs. NHE) already shown in Figure 5(a). We noted that $H_2$ was produced over Au(1.0)/$CeO_2$:Sr(0.05)-Pt(0.5), indicating that electrons injected into the CB of $CeO_2$:Sr(0.05) at −0.0090 V vs. NHE reduce $H^+$ to $H_2$ with the aid of the Pt co-catalyst. The difference in the results for Au(1.0)/$CeO_2$-Pt(0.5) and Au(1.0)/$CeO_2$:Sr(0.05)-Pt(0.5) indicates that the position of the CB of a semiconductor is an important factor for $H_2$ evolution over an Au-semiconductor plasmonic photocatalyst as well as for $H_2$ formation over semiconductors utilizing band-gap excitation of electrons.

The rate of $H_2$ formation increased because the more negative potential of electrons in the CB has an advantage for $H_2$ evolution and reached a maximum (5.6 μmol $h^{-1}$, Figure 6)

at x = 0.25. Further increase in x decreased the rate, suggesting that injection of electrons into the CB gradually becomes difficult; however, evolution of $H_2$ for the x= 0.40 sample indicates that hot electrons can be injected from Au particles into the CB of CeO2:Sr(0.40), of which the potential is −0.61 V vs. NHE. No $H_2$ was produced over Au(1.0)/$CeO_2$:Sr(0.50)-Pt(0.5). This also provides important information that the maximum potential of hot electrons provided by SPR of Au particles under visible light irradiation is lower than the position of $E_{CB}$ of $CeO_2$:Sr(0.50) (−1.49 V vs. NHE). From the results, we concluded that the limit position of the CB of semiconductors accepting hot electrons from Au particles lies between −0.61 V and −1.49 V vs. NHE.

### 3.4 Platinum-free $H_2$ evolution over Au/$CeO_2$:Sr(x)

In the previous section, Pt cocatalyst was loaded on Au/$CeO_2$:Sr(x) samples because Pt often accelerates photocatalytic $H_2$ evolution. Kudo *et al*. reported that cocatalyst-free $H_2$ evolution is possible if the potential of photogenerated electrons (in other words, the CB position of the semiconductor) is sufficiently negative for the production potential of $H_2$ (0 V vs. NHE)[24]. Since the position of the VB of metal oxide semiconductors is mostly determined by the O2p orbital, candidates of metals for an $H_2$-producing metal oxide photocatalyst without the aid of a co-catalyst are limited to metals having a sufficiently negative position of the d orbital. Therefore, semiconductor photocatalysts having a sufficient negative potential are limited to wide band-gap metal oxides requiring irradiation of UV light of which the wavelength is shorter than λ= 300 nm. In contrast to metal oxide semiconductors, the CB positions of some of the Au/$CeO_2$:Sr(x) samples were sufficiently negative for $H_2$ production despite the fact that hot electrons can be injected into the CB under visible light irradiation. Therefore, we reached the idea that Pt-free $H_2$ production is possible over Au/$CeO_2$:Sr(x) under visible light irradiation and we carried out photocatalytic reaction of 2-propanol in aqueous suspensions of Pt-free Au/$CeO_2$:Sr(x) samples.

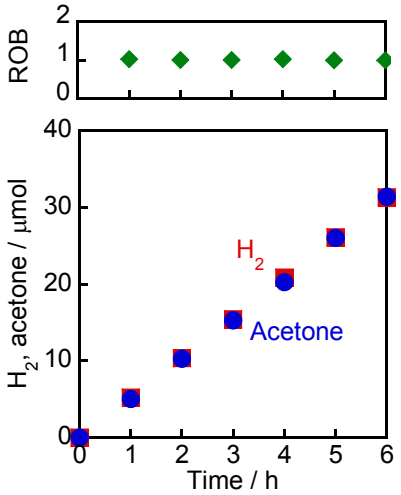


Figure 7 Time courses of formation of $H_2$ and acetone from 2-propanol over Au(1.0)/$CeO_2$:Sr(0.25) under irradiation of visible light from a Xe lamp with a Y48 cut filter.

Figure 7 shows time courses of the formation of $H_2$ and acetone from 2-propanol in an aqueous suspension of Au(1.0)/$CeO_2$:Sr(0.25) under visible light irradiation. As expected, Pt-free Au(1.0)/$CeO_2$:Sr(0.25) continuously produced $H_2$ and acetone with a molar ratio of 1:1, and the reaction rate (5.2 μmol $h^{-1}$) was almost the same as the rate (5.6 μmol $h^{-1}$) of the platinized sample (Au(1.0)/$CeO_2$:Sr(0.25)-Pt). To investigate the effect of a Pt co-catalyst on $H_2$ evolution, Pt-free Au/$CeO_2$:Sr samples were used for photocatalytic reaction of 2-propanol, and the results are shown in Figure 8.

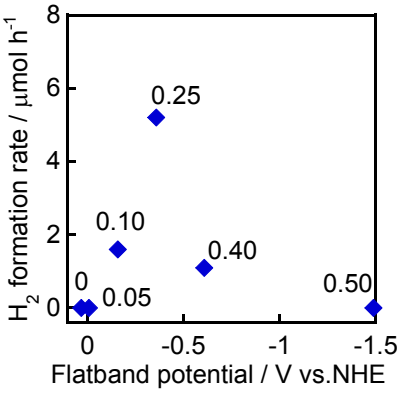


Figure 8 Effect of Pt cocatalyst on $H_2$ formation rate of a Pt-free Au(1.0)/$CeO_2$:Sr(x) plasmonic photocatalyst. Values in the figure show mole fractions of $Sr^{2+}$ (x).

In the case of Pt-free Au(1.0)/$CeO_2$:Sr(0.05), no $H_2$ was produced, although platinized Au(1.0)/$CeO_2$:Sr(0.05) produced $H_2$ under the same conditions. The contrasting results (effect of a Pt cocatalyst) were caused by the position of the CB of $CeO_2$:Sr(0.05) (−0.0090 V vs. NHE), which is very close to the value to 0 V required for $H_2$ evolution. This result indicates that Pt worked as an effective cocatalyst for $H_2$ evolution over semiconductors of which the position of the CB is very close to 0 V such as Au(1.0)/$CeO_2$:Sr(0.05). Figure 8 shows that other Au/$CeO_2$:Sr samples produced $H_2$ without the aid of a Pt cocatalyst, and the rates were almost same as those of the platinized Au/$CeO_2$:Sr samples, *i.e.*, Au(1.0)/$CeO_2$:Sr(0.10) did not need the aid of a Pt cocatalyst any more for production of $H_2$ by electrons injected into the CB. Therefore, we concluded that the minimum potential of the CB for which production of $H_2$ over Pt-free Au/$CeO_2$:Sr is possible lies between −0.0090 V and −0.16 V vs. NHE.

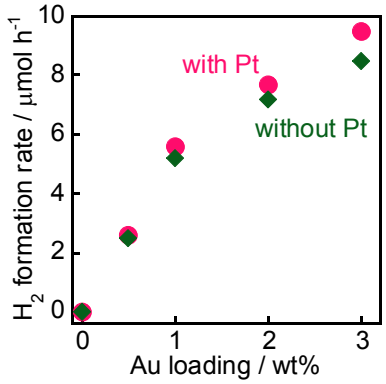


Figure 9 Effect of amount of Au loading on $H_2$ formation rate of Pt-free Au(1.0)/$CeO_2$:Sr(0.25) and Au(1.0)/$CeO_2$:Sr(0.25)-Pt plasmonic photocatalysts.

### 3.5 Effect of Au content on $H_2$ evolution

Figure 9 shows the effect of the amount of Au on $H_2$ evolution over Au/$CeO_2$:Sr(0.25) with and without a Pt cocatalyst. The rate of $H_2$ formation increased with an increase in Au loading and reached 9.5 μmol $h^{-1}$ at 3.0 wt% over platinized Au/$CeO_2$:Sr(0.25), although the rate tended to be saturated. As expected, production of $H_2$ was observed over Pt-free Au/$CeO_2$:Sr(0.25) and the rate increased with increasing Au content as in the case of platinized Au/$CeO_2$:Sr(0.25). We noted that the difference in rates of $H_2$ formation over platinized and Pt-free Au/$CeO_2$:Sr(0.25) became large, *i.e.*, Pt loading was effective for Au/$CeO_2$:Sr(0.25) having a larger Au content to sufficiently produce $H_2$. In the case of $CeO_2$:Sr(0.25) having a larger Au content, a large amount of electrons was injected from Au into the CB of $CeO_2$:Sr(0.25). These results indicate that the function of a Pt cocatalyst was observed only under an electron-rich condition.

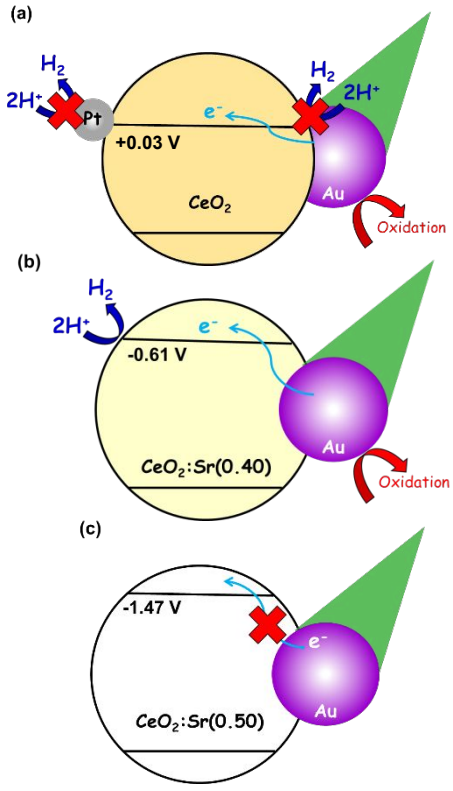


Figure 10 Expected electron transfer from Au nanoparticle to the CB of (a) Au/$CeO_2$, (b) Au/$CeO_2$:Sr(0.40) and (c) Au/$CeO_2$:Sr(0.50) under visible light irradiation, and (b) cocatalyst-free plasmonic $H_2$ production over Au/$CeO_2$:Sr(0.40).

## Conclusions

$CeO_2$:Sr samples having various $Sr^{2+}$ mole fractions(x) were prepared by a solid state reaction. Impedance measurement of these samples indicated that the values of $E_{FB}$ of $CeO_2$:Sr(x) gradually shifted negatively with an increase in x. In other words, $CeO_2$:Sr(x) samples having different $E_{CB}$ from −0.0090 V to −1.49 V (vs. NHE) were successfully prepared by changing x of $CeO_2$:Sr(x). By using the PD method and the CPH method, Pt and Au particles were successfully loaded on $CeO_2$ and $CeO_2$:Sr(x) samples, respectively. In the photocatalytic reaction of 2-propanol under irradiation of visible light, electrons were injected from Au particles into the CB of the semiconductor, and it was shown that the position (positive or negative) of the CB of the semiconductor is important for $H_2$ formation, *i.e.*, no $H_2$ was evolved over Au(1.0)/$CeO_2$-Pt(0.5) (+0.031 V vs. NHE) (Figure 10(a)), while $H_2$ was produced over Au(1.0)/$CeO_2$:Sr(0.05)-Pt(0.5) (−0.0090 V vs. NHE). The rate of $H_2$ evolution increased with the negative shift in the position of the CB because a more negative potential of electrons in the CB has an advantage for $H_2$ evolution. Electrons could be injected from Au particles into the CB of $CeO_2$:Sr(0.40), of which the potential is −0.61 V vs. NHE (Figure 10(b)), although the efficiency became lower. Electrons were not injected into the CB of $CeO_2$:Sr(0.50) (−1.49 V vs. NHE) any more (Figure 10(c)), indicating that the limit position of the CB of semiconductors accepting hot electrons from Au particles lies between −0.61 V and −1.49 V vs. NHE. Since the CB positions of some of Au/$CeO_2$:Sr(x) samples [x= 0.10. 0.25, 040] were sufficiently negative for $H_2$ production, Pt-free Au(1.0)/$CeO_2$:Sr(x) continuously produced $H_2$ (Figure 10(b)) at a rate that was almost the same as that for platinized samples. The function of a Pt co-catalyst was observed only under an electron-rich condition over $CeO_2$:Sr having a large Au content.

## Conflicts of interest

There are no conflicts to declare.

## Acknowledgements

This work was partly supported by JSPS KAKENHI Grant Numbers 17H03462 and 17H04967 and the Precursory Research for Embryonic Science and Technology (PRESTO), supported by the Japan Science and Technology Agency (JST). This work was also supported by MEXT-Supported Program for the Strategic Research Foundation at Private Universities 2014-2018, subsidy from MEXT and Kindai University. A.T. is grateful for financial support from the Faculty of Science and Engineering, Kindai University and the Nippon Sheet Glass Foundation for Materials Science and Engineering.

## References

1 H. Park, Y. Park, W. Kim and W. Choi, *Journal of Photochemistry and Photobiology C: Photochemistry Reviews* 2016, **15**, 1.

2 (a) W. Macyk, G. Burgeth and H. Kisch, *Photochem. Photobiol. Sci.*, 2003, **2**, 322; (b) S. Kitano, N. Murakami, T. Ohno, Y. Mitani, Y. Nosaka, H. Asakura, K. Teramura, T. Tanaka, H. Tada, K. Hashmoto and H. Kominami, *J. Phys. Chem. C*, 2013, **117**, 11008.

3 H. Irie, K. Kamiya, T. Shibanuma, S. Miura, D. A. Tryk, T. Yokoyama and K. Hashimoto, *J. Phys. Chem. C*, 2009, **113**, 10761.

4 (a) S. Ikeda, C. Abe, T. Torimoto and B. Ohtani, *J. Photochem. Photobiol., A*, 2003, **160**, 61; (b) T. Kamegawa, H. Seto, S. Matsuura and H. Yamashita, *ACS Appl. Mater. Interfaces*, 2012, **4**, 6635; (c) H. Kominami, S. Kitagawa, Y. Okubo, M. Fukui, K. Hashimoto and K. Imamura, *Phys. Chem. Chem. Phys.*, 2016, **18**, 16076.
5 E. Kowalska, R. Abe and B. Ohtani, *Chem. Commun.*, 2010, **46**, 815.
6 (a) E. Kowalska, O. O. P. Mahaney, R. Abe and B. Ohtani, *Phys. Chem. Chem. Phys*., 2010, **12**, 2344; (b) H. Kominami, A. Tanaka and K. Hashimoto, *Chem. Commun*., 2010, **46**, 1287; (c) H. Kominami, A. Tanaka and K. Hashimoto, *Appl. Catal. A*, 2011, **397**, 121; (d) A. Tanaka, K. Hashimoto and H. Kominami, *ChemCatChem*, 2011, **3**, 1619; (e) A. Tanaka, A. Ogino, M. Iwaki, K. Hashimoto, A. Ohnuma, F. Amano, B. Ohtani and H. Kominami, *Langmuir*, 2012, **28**, 13105.
7 (a) S. Naya, M. Teranishi, T. Isobe and H. Tada, *Chem. Commun.*, 2010, **46**, 815; (b) A. Tanaka, K. Hashimoto and H. Kominami, *Chem. Commun*., 2011, **47**, 10446; (c) A. Tanaka, K. Hashimoto and H. Kominami, *J. Am. Chem. Soc*., 2012, **134**, 14526.
8 (a) C. G. Silva, R. Juarez, T. Marino, R. Molinari and H. Garcia, *J. Am. Chem. Soc*., 2011, **133**, 595; (b) H. Yuzawa, T. Yoshida and H. Yoshida, *Appl. Catal. B*, 2012, **115**, 294; (c) A. Tanaka, S. Sakaguchi, K. Hashimoto and H. Kominami, *Catal. Sci. Technol*., 2012, **2**, 907; (d) A. Tanaka, S. Sakaguchi, K. Hashimoto and H. Kominami, *ACS Catal*., 2013, **3**, 79.
9 X. Ke, X. Zhang, J. Zhao, S. Sarina, J. Barry and H. Zhu, *Green Chem*., 2013, **15**, 236.
10 A. Tanaka, K. Teramura, S. Hosokawa, H. Kominami and T. Tanaka, *Chem. Sci*., 2017, **8**, 2574.
11 J. Xue, S. Ma, Y. Zhou, Z. Zhang and M. He, *ACS Appl. Mater. Interfaces*, 2015, **7**, 9630.
12 A. Tanaka, K. Hashimoto and H. Kominami, *J. Am. Chem. Soc*., 2014, **136**, 586.
13 S. Kim, Y. Yu, S. Jeong, M. G. Lee, H. W. Jeong, Y. M. Kmon, J. M. Baik, H. Park, H. W. Jang and S. Lee, *Catal. Sci. Technol.*, 2018, **8**, 3759.
14 L. Kavan, M. Gra¨tzel, S. E. Gilbert, C. Klemenz and H. J. Scheel, *J. Am. Chem. Soc.*, 1996, **118**, 6716.
15 K. Kadowaki N. Saito, H. Nishiyama and Y. Inoue, *Chem. Lett*., 2007, **36**, 3.
16 Y. Inoue, *Energy Environ. Sci*., 2009, **2**, 364.
17 G. Frens, *Nature Phys. Sci.*, 1973, **241**, 20.
18 W-J Chun, A. Ishikawa, H. Fujisawa, T. Tanaka, J. Kondo, M. Hara, M. Kawai, Y. Matsumoto and K. Domen, *J. Phys. Chem. B*, 2003, **107**, 1798.
19 S. Iguchi, S. Kikkawa, K. Teramura, S. Hosokawa and T. Tanaka, *Phys. Chem. Chem. Phys.*, 2016, **18**, 13811.
20 R. Beranek, *Adv. Phys. Chem*., 2011, **2011**, 1.
21 S. Yabe, M. Yamashita, S. Momose, K. Tahira, S. Yoshida, R. Li, S. Yin and T. Sato, *International Journal of Inorganic Materials*, 2001, **3**, 1003.
22 H. Hou, K. Watanabe, H. Furuno, M. Nishikawa and N. Saito, *Chem. Lett*., 2019, **48**, 200.
23 M.I. Sosulnikov and Y. A. Teterin, *J.Electron. Spectrosc. Relat. Phenom.,* 1992, **59**, 101.
24 (a) H. Kato and A. Kudo, *Catal. Lett*., 1999, **58**, 153; (b) H. Kato, K. Asakura and A. Kudo, *J. Am. Chem. Soc.*, 2003, **125** 3082.

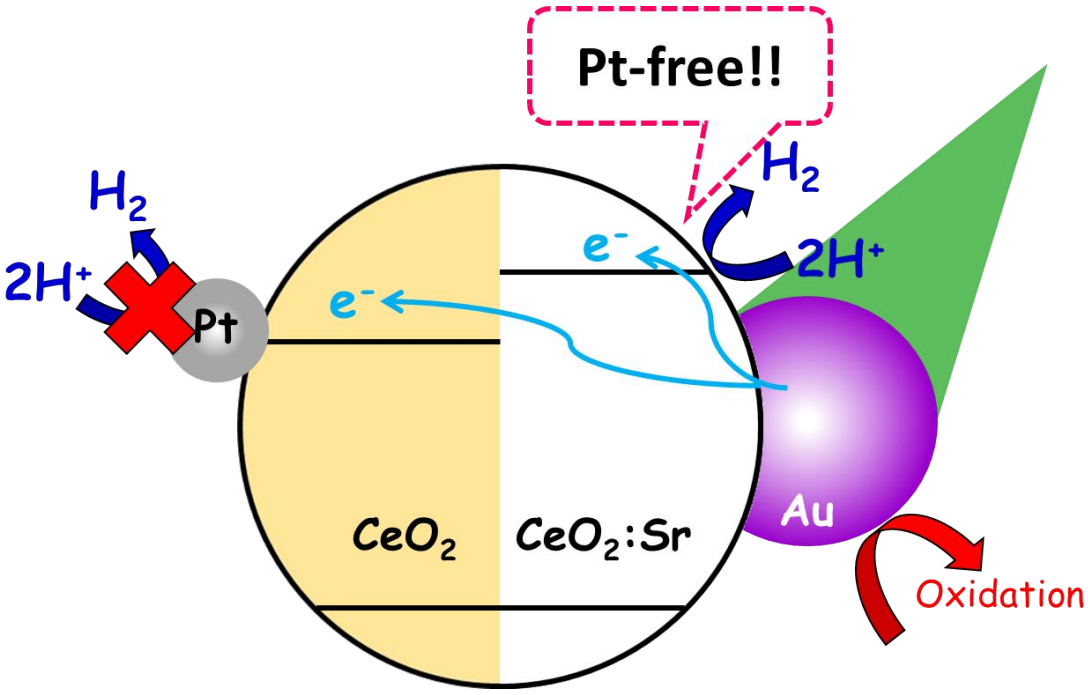


Au/$CeO_2$:Sr plasmonic photocatalysts produced $H_2$ without the aid of a cocatalyst due to the sufficiently negative potential of electrons injected into the CB of $CeO_2$:Sr.